Ground subsidence monitoring with SAR interferometry techniques in the rural area of Al Wagan, UAE

Nikolaos Liosis[1]*, Prashanth Reddy Marpu[1], Kosmas Pavlopoulos[2] and Taha Ouarda[3]

[1]*Institute Center for Water and Environment, Khalifa University of Science and Technology, Masdar Institute, Masdar City, P.O. Box 54224, Abu Dhabi, United Arab Emirates;* [2]*Department of Geography and Planning, Paris-Sorbonne University Abu Dhabi, P.O. Box 38044 AD UAE;* [3]*Laboratoires d'Hydraulique Institut National de la Recherche Scientifique Centre Eau Terre Environnement 490, rue de la Couronne Québec (Québec) G1K9A9 Canada;*

*Corresponding author. Email: nliosis@masdar.ac.ae

Abstract

In this work, we investigate the past and present land deformation in Al Wagan area in the United Arab Emirates. The area is primarily an agricultural region where dependence on groundwater is documented. Such a reliance on ground water resources in a region which is characterized by very low precipitation can lead to significant land subsidence as was observed in this study which identified fast and localized deformation trends. The quantification of terrain distortions of large magnitude and small amplitude in this area with SAR Interferometry is a challenging task using moderate resolution data due to the incoherent surface background. Even though SAR acquisitions were sparse over this region, the available ENVISAT, ALOS and Sentinel-1A imagery was analysed with differential interferometry and the Small Baseline Subset technique in order to provide fair estimates about the evolution of the deformation pattern in a limited area. The depletion of the aquifer resources which is confirmed from groundwater level data is speculated to be the most probable cause. However these assumptions require further investigation in order to discover a remediation for this problem.

Keywords: SAR Interferometry; SBAS; subsidence; groundwater; UAE

Introduction

Excessive groundwater extraction from the subsurface may lead to the depletion of the aquifer's natural resources, which potentially results in ground surface subsidence phenomena. The agriculture sector of the United Arab Emirates (UAE) has been expanding since the 1990s (Statistics Centre of Abu Dhabi, 2014), but since all these farms are situated in an arid region with a hot desert climate and extremely sparse precipitation events, they mostly relied on groundwater for their viability (Environmental Agency of Abu Dhabi, 2009). The direct implications of this are the diminishing natural aquifer resources of the UAE, which has already been analysed in another study (Gonzalez et al., 2016), the degradation of the water quality (Vrba, 2003; Al-Naeem, 2014) and the occurrence of localized terrain subsidence (Holzer and Galloway, 2005).

Differential Synthetic Aperture Radar (SAR) Interferometry (DInSAR) is one of the most effective remote sensing methods to quantify terrain distortions related to various causes over a large spatial scale (Bürgmann et al., 2000; Ferretti, 2014). The multi-temporal stacking techniques that have been developed in the past two decades, like Persistent Scatterers (PS) (Ferretti et al., 2001; Hooper et al., 2004) and Small Baseline Subset (SBAS) (Berardino et al., 2002; Lanari et al., 2004), are capable of providing accurate estimations of the displacement time series and the deformation velocities, with the latter method being more suitable for rural regions as it is based on identifying Distributed Scatterers (DS) that are more common in natural environments in a stack of small baseline interferograms. There already exist numerous studies where groundwater related subsidence phenomena were successfully assessed with SBAS techniques (Chaussard et al., 2014; Kim et al., 2015; Artesea et al., 2016). However, the accuracy and the reliability of the results is affected by temporal decorrelation in rural areas where incoherent surface types, like sand and vegetation are the dominant land covers (Bamler and Hartl, 1998; Massonnet and Feigl, 1998).

DInSAR applications are very sparse in the UAE mainly due to the extended presence of the sandy geological background which significantly degrades the performance of the process and the reliability of the final outputs. A previous study had demonstrated the application of SBAS over an extended area of the Eastern part of the UAE focusing on the most coherent parts and providing rough indications about the locations of particular ground distortion zones (Cantone et al., 2013). However, to the authors' knowledge, there are no existing studies attempting to monitor localized surface deformations in the UAE at small scales. The major challenge in this rural area where the subsidence phenomena were extremely fast and localized was to define the optimum data resolution that allowed the detection and depiction of the real deformation magnitude in the presence of high decorrelation noise.

This work is part of the study currently being conducted in the UAE aiming to detect regions affected by subsidence phenomena induced by subsurface resources exploitation and to provide quantitative estimations about the spatiotemporal patterns of the terrain displacements. The objective of the present work is to analyse the observations obtained by conventional DInSAR and SBAS techniques and to demonstrate that despite the presence of low coherence that obstructs the interferometric processing, reliable results may still be obtained to provide a comprehensive overview of the subsidence phenomenon in the study area over a larger spatial extent than is possible by sparse permanent GPS stations.

Study Area

Al Wagan is located on the eastern part of the Abu Dhabi Emirate, approximately 65 kilometres southwest of the city of Al Ain at the borders with Oman. Figure 1a depicts the study area along with the locations of monitored wells from the Environmental Agency of Abu Dhabi (EAD). It is a hot and arid region at the edge of the Rub' al Khali desert with a generally flat terrain - except for the star dunes - at an average altitude of 170 meters. The surrounding area of this sparsely populated town facilitates many farms at the west side of the borders which unequally spread up to 18 kilometres towards the desert gradually fading out. The farms along with other vegetated areas cover around 71 km^2 over a total area of approximately 357 km^2.

The borders of the UAE with Oman at the study area roughly depict the transition from the fluvial deposits in the east to the Aeolian deposits to the west. The geological background of the north part of the region where the main settlement is sited consists of fluvial quaternary deposits which are composed of a mixture of sandstone, conglomerates and siltstone (Hili formation), formed by torrent activity originating from the Omani mountains. The central and southern parts are mainly covered by low and star dunes of sandy material transferred by aeolian processes. The heterogeneity of the local geology shown in figure 1b is clearly visible in radar and optical satellite imagery and sporadic shifts between these two main background types are not uncommon. The geological map of the area is not totally reflected on the land use map (figure 1c), implying that the farms are not located exclusively on the alluvial fans but on the sand deposits as well.

There were no active faults in the study area observed in the geological maps neither mentioned in literature. The nearest regions that were affected by active tectonism in the studied period were the Fujairah Mountains and the Musandam Peninsula (Yagoub, 2015). Therefore it was considered in this study that the effects of earthquakes on surface deformations were negligible and they were not taken into account.

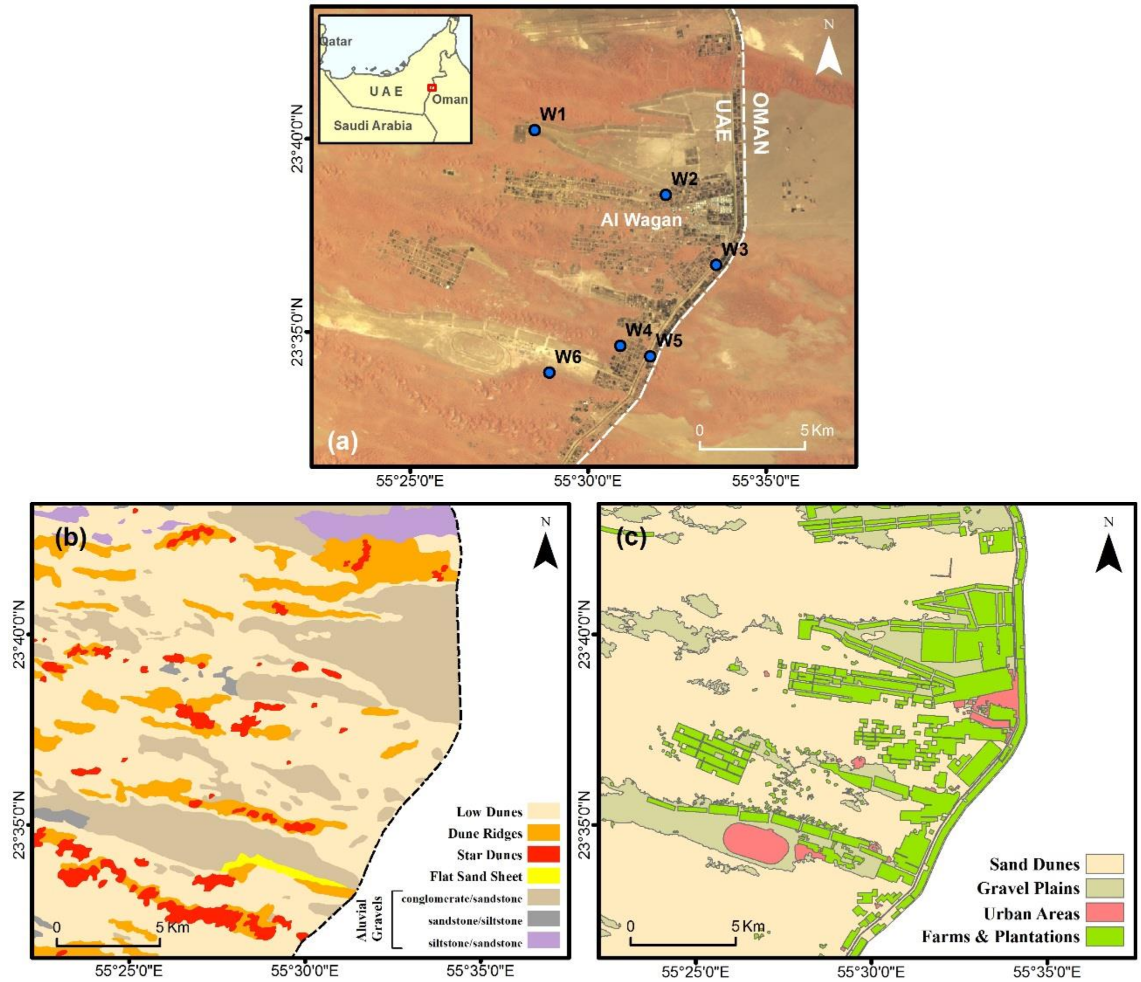

Figure 1. a) Landsat 8 composite image (bands 4, 3, 2) of the study area dated 26/5/2017. b) Geological map (BGS) c) Generalized land cover map (EAD).

Data

The interferometric analysis was performed with the use of the freely available C-band and L-band SAR data covering the study area. Two C-band image stacks acquired from the ENVISAT satellite by the Advanced Synthetic Aperture Radar (ASAR) sensor were obtained from the European Space Agency (ESA). The descending stack consists of 32 acquisitions covering the period 7/8/2003 – 22/4/2010, while the ascending includes only 10 images from the period 3/4/2007 – 14/10/2008. Other C-band data used in this study were the available Sentinel-1A acquisitions over the area of interest, but the sparsity of the data did not allow a proper time series analysis. Three SAR acquisitions were used for differential interferogram generation dated 18/2/2016, 2/12/2016 and 8/3/2017. The L-band data were also sparse over this region, consisting of 7 ALOS PALSAR acquisitions from the period 5/8/2007 – 10/8/2009 obtained from the Alaska Satellite Facility (ASF). The general characteristics of these radar data are presented in table 1.

Table 1. Main characteristics of the SAR data used in the study.

Sensor	Number of images	Pass	Track/Frame	Acquisition Mode	Polarization
ENVISAT/ASAR	32	Descending	435/3123	IW-IM	VV
ENVISAT/ASAR	10	Ascending	13/459	IW-IM	VV
ALOS/PALSAR	4	Ascending	460/567	FBD	HH-HV
ALOS/PALSAR	3	Ascending	460/567	FBS	HH
Sentinel-1A	3	Ascending	130	IW	VV-VH

The topographic phase removal was performed with the 3 arcsecond Digital Elevation Model (DEM) of the Shuttle Radar Topography Mission (SRTM). Other data that were used include the geological map of the area produced by the British Geological Survey (BGS) under contract from the Ministry of Energy of the UAE, the Terrestrial Habitat map of the UAE and the groundwater levels from the monitored wells of the study area obtained from the Environmental Agency of Abu Dhabi (EAD) in the period 5/3/2000 – 9/9/2015.

Methods

DInSAR relies on the isolation of the deformation phase component which corresponds to the terrain movements between the two SAR acquisitions of similar geometry. The Single Look Complex (SLC) images of each stack were coregistered on a single master scene in order to compute the interferograms. Due to the flat relief of the study area the SRTM DEM of 90 m. resolution was considered adequate for subtraction of the local topography, since differences between trials with the ASTER and the 30 m. resolution SRTM DEMs were insignificant. The Goldstein method was used to apply frequency domain phase filtering to the differential interferograms (Goldstein and Werner, 1998) with small windows in order to avoid aliasing fast deformation fringes, at the expense of preserving a lot of decorrelation noise in the final outputs. After the phase unwrapping stage (Pepe and Lanari, 2006), orbital refinement was performed for estimation and removal of residual phase ramps from the unwrapped interferometric stack by selecting ground control points common for all the generated interferograms.

The SBAS technique is based on generating and stacking a series of interferograms with small perpendicular baselines in order to reduce the spatial decorrelation effects. Therefore, the DInSAR process was applied to interferograms that satisfied certain temporal/perpendicular orbit criteria depending on the monitored surface types, the critical baseline and the relative space-time dispersion of the acquisitions in each stack. At the first inversion of the SBAS algorithm a primary estimate of the mean velocity field was obtained by applying a low degree displacement model to the unwrapped phases. This low pass deformation component along with possible topographic remnants was subtracted from the wrapped interferograms. Subsequently, the residual phase was unwrapped and added back to the subtracted deformation signals (Berardino et al., 2002).

In the second step the refined unwrapped interferograms were inverted with a Singular Value Decomposition (SVD) approach in order to derive the time series of the displacements (Lanari et al., 2007). The atmospheric signals were removed with low pass spatial and high pass temporal filtering operations (Ferretti et al., 2000) and the final deformation history and velocity of the multi-temporally coherent pixels was extracted along with the topographic residuals between the DEM and the actual ground surface. The results were geocoded in UTM zone 40N projected coordinate system and the data processing was mainly performed with Sarscape software. The general workflow of the interferometric processes applied in this study is summarized in figure 2.

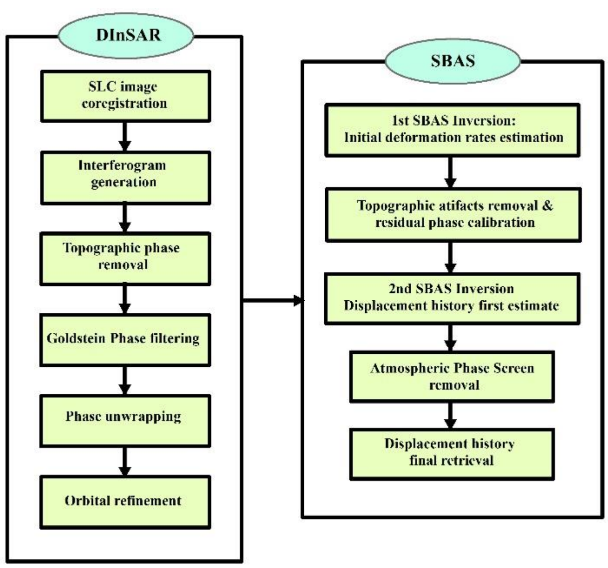

Figure 2. Flow chart of the interferometric processes.

Interferometric processing and results

ENVISAT data

Since the acquisitions of the descending stack were temporally irregular with a gap period from July 2004 to February 2006 (figure 4b), the thresholds for interferogram generation were set to 800 days temporal / 360 m. perpendicular baseline in order to avoid underlaps in the stack. The coherence maps showed that the alluvial gravels were remaining generally coherent for more than two years in short baseline interferometric pairs, but the coherence of the sand dune areas was completely lost within 35 days. The block structured farms located in the sandy areas maintained their coherence at moderate levels for 100 - 150 days.

Despite the low phase signal quality the differential interferograms revealed a fast subsidence pattern extended throughout the whole farmland area with the deformation magnitude along the Line-Of-Sight (LOS) peaking at several points within the region, especially along the west side of the highway that links the border settlements. In the central and south regions, the deformations were even greater. But this observation relied only on small temporally separated pairs as temporal decorrelation prevented from obtaining long term estimations. A seasonal variation was also observed as the summer period pairs tended to exhibit larger displacement signals than those of the winter season, reaching almost one fringe per month south of the town of Al Wagan. If the observed subsidence was related to groundwater pumping, the increased water demands of agriculture in a desert environment during the hot and dry periods could explain this phenomenon. These primary observations were consistent in all the temporally coherent interferograms of both the ascending and the descending stacks, which reinforced the initial assumption of a fast subsidence phenomenon.

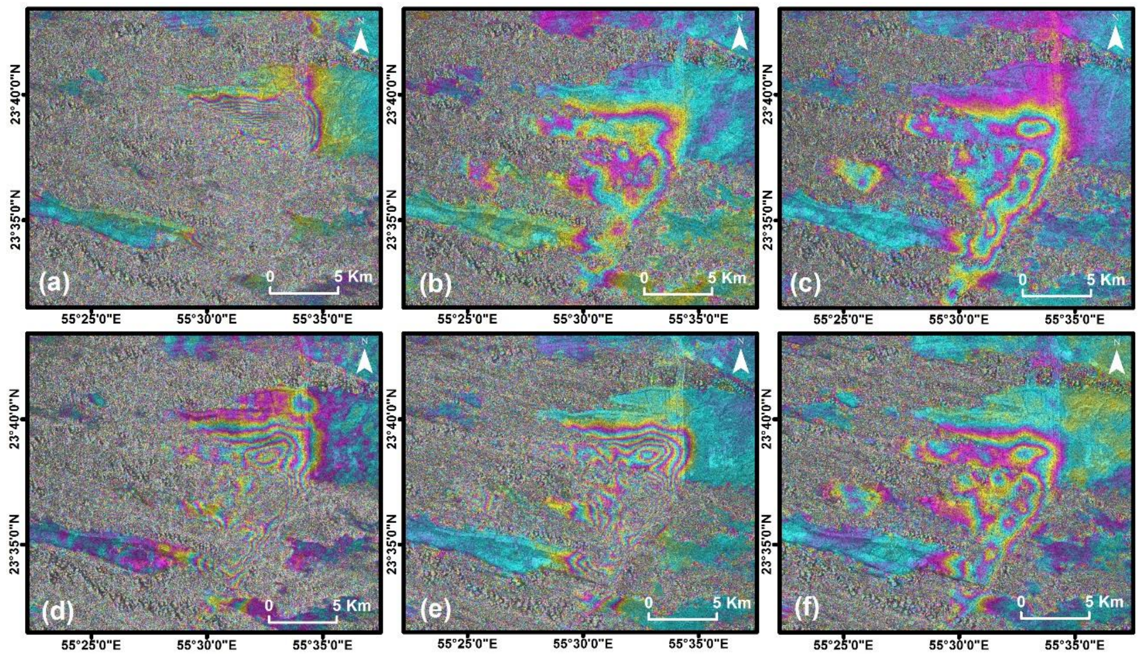

Figure 3. Differential interferograms from ENVISAT pairs. a) From descending pair 3/4/2004 - 9/3/2006, where temporal and fast fringes decorrelation are dominant in long time spans. b) Descending pair 29/11/2007 - 17/4/2008, indicative of the lower fringe rates in the winter seasons. c) Descending pair of 17/4/2008 – 26/6/2008. d) Descending pair 7/5/2009 - 11/2/2010, where the deformation pattern is clear despite the decorrelation noise. e) Ascending pair 3/4/2007 – 12/2/2008. f) Ascending pair 8/1/2008 – 27/5/2008.

The detection of this fast subsidence pattern depended on the maximum detectable deformation gradient, which theoretically is one fringe per pixel (Massonnet and Feigl, 1998). Since in reality this threshold is significantly lower due to the presence of decorrelation noise in low coherent areas (Baran et al., 2005), and fast fringes decorrelation was observed in all the interferograms of more than two years separation, the images were multilooked 1 x 5 (range x azimuth). For larger factors, the deformation pattern became undetectable or ambiguous even in temporally adjacent pairs.

In order to obtain an initial estimation of the deformation velocities, interferometric stacking was applied (Strozzi et al., 2001) after the phase unwrapping stage with pairs of short perpendicular baselines (< 250 m). Due to temporal decorrelation and phase unwrapping failures the reliability of the output linear deformation velocities was compromised, however the areas of stability were delineated for subsequent reference point selections.

The interferograms of the descending stack were then used as inputs for the SBAS algorithm. After discarding the pairs with significant unwrapping errors, 84 interferograms were inverted in order to extract the displacement history and velocities of the multi-temporally coherent points. The relative time-baseline position of the images is shown in figure 4b. The resulting deformation maps showed that cumulative subsidence exceeded 1 meter and LOS displacement rates reached -18 cm/year in the most affected areas during the sampling period, with the time series exhibiting a small seasonal effect. However, the coherent pixel grid was sparse at the central and south parts of the study area where subsidence appeared larger in the short temporal baseline interferograms, exhibiting displacements equal or lower than those of the north part. Decorrelation and unwrapping errors prevented from obtaining accurate estimates in those regions.

Figure 4a depicts the vertical deformation rates in the study area (valid under the assumption of negligible horizontal component). Point P1 is located in the northernmost part of the region where even though displacement rates were low, an accelerating subsidence trend was observed after 2007. P2 is sited in the fast subsiding area near the town at the local deformation maximum, while W2 is a monitored well within the same area. P3 and P4 are representative points of the central and south subsiding regions respectively. Even though according to the displacement history of figure 4c they exhibit lower or equal deformations with point P2, it is noted that coherence levels were marginal in these areas and a sufficient density of measure points was not achieved.

As a general observation, the linear model that was applied to the displacement velocities could roughly capture the seasonal behaviour of the ground deformations. It is also noted that a quadratic model was a more appropriate fit in the southern region proximate to P4 as it was in the area of P1, with the subsidence phenomenon slightly accelerating after 2006. In either case, it is not certain whether this was due to the higher frequency of acquisitions after that year (figure 4b), since the large temporally separated pairs of the preceding gap period included many phase inconsistencies in the low coherent areas.

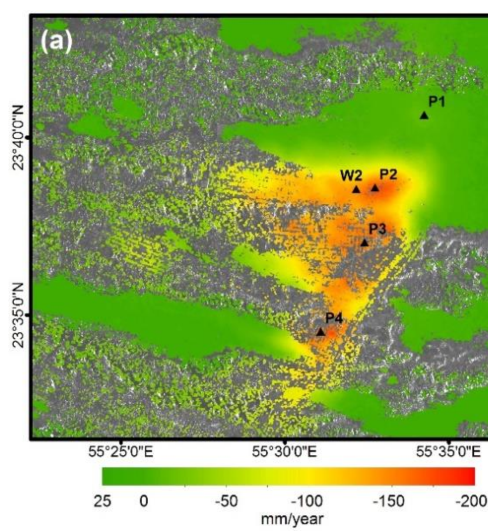

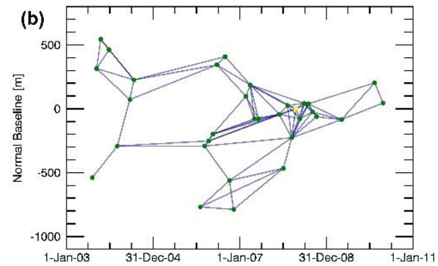

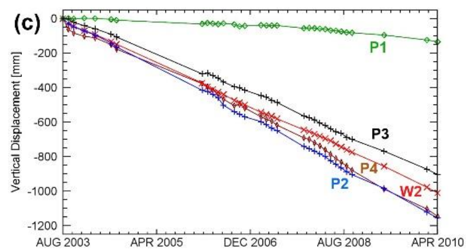

Figure 4. a) Vertical displacement velocities of the period 2003 - 2010. b) Time position plot of the descending stack images, where nodes and arcs represent scenes and interferograms respectively. c) Displacement history of selected points in the study area.

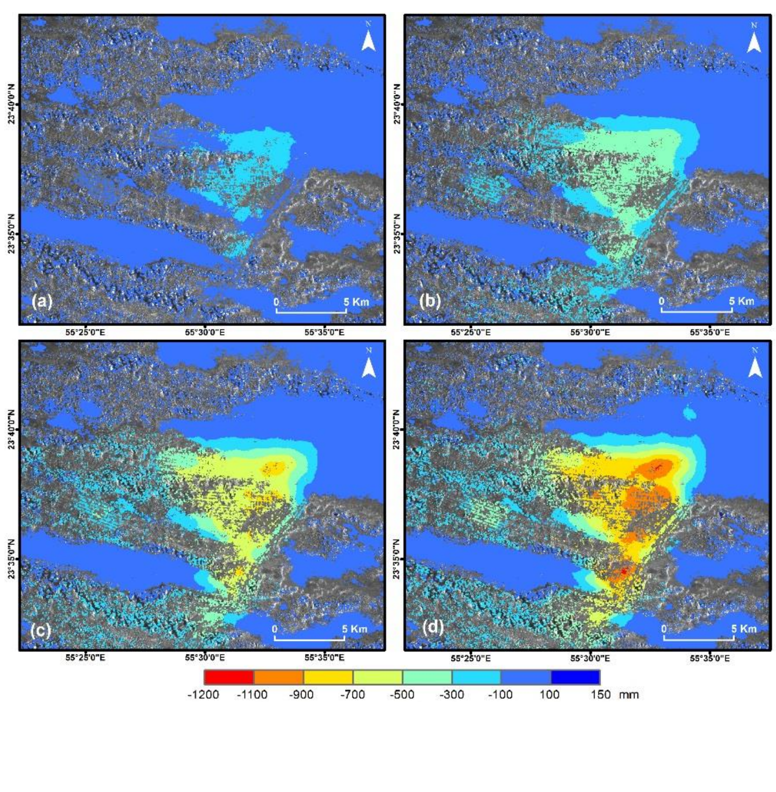

Figure 5. Evolution of the LOS deformation pattern obtained from the descending acquisitions. a) 7/8/2003 - 22/7/2004. b) 7/8/2003 - 22/6/2006. c) 7/8/2003 - 22/5/2008. d) 7/8/2003 - 22/4/2010.

The SBAS technique was applied with 20 interferograms of the ascending stack within 400 days temporal separation and 330 m. maximum normal baseline for comparison with the results obtained from the descending stack. The generated maps replicated the ground distortion pattern of the previous implementation which verified that the vertical movements were dominant, considering the similar incident angle of the ascending and descending acquisitions. The cumulative LOS displacements derived from the two stacks were comparable in the northern area during similar observation periods.

However, in the central and southern regions of the study area, where the multitemporal coherence was increased in the ascending stack, the deformations of the commonly coherent pixels appeared significantly larger than those estimated from the descending stack. These local deviations were mostly attributed to phase inconsistencies induced by decorrelation noise in the interferograms of the descending stack rather than to a horizontal component of the terrain movements. The coherence maps of both stacks are shown in figure 6.

The comparison of the cumulative LOS displacements between the two stacks in the sampling period of the ascending acquisitions is demonstrated in figures 7a and b. Figure 7d illustrates the vertical displacement history of the selected points in the study area after the application of a linear model to the subsidence rates. Points P1, P2 and W2 follow the same pattern as derived from the descending stack. The estimated displacements in these areas were precisely estimated due to the alluvial sediment background, which was adequately coherent in both stacks. Points P3 and P4 exhibited faster subsidence rates than P2, confirming the primary estimate from the differential interferograms of both stacks that these regions were subsiding faster than the northern area.

On the other hand, the ascending stack could not provide precise estimates due to the sparsity of acquisitions whereas local phase unwrapping failures in low coherent regions were neither absent in the ascending pairs. Indicatively, the (multitemporal) coherence values of points P3 and P4 were 0.48 and 0.26 respectively contrasted to 0.23 for both points in the descending stack. Even though the time span of the acquisitions included two summer periods, higher order models were not applied due to the extended low coherent regions and the small number of scenes. Nevertheless, this short time interval was considered too short to draw safe conclusions about the exact deformation behaviour of these areas.

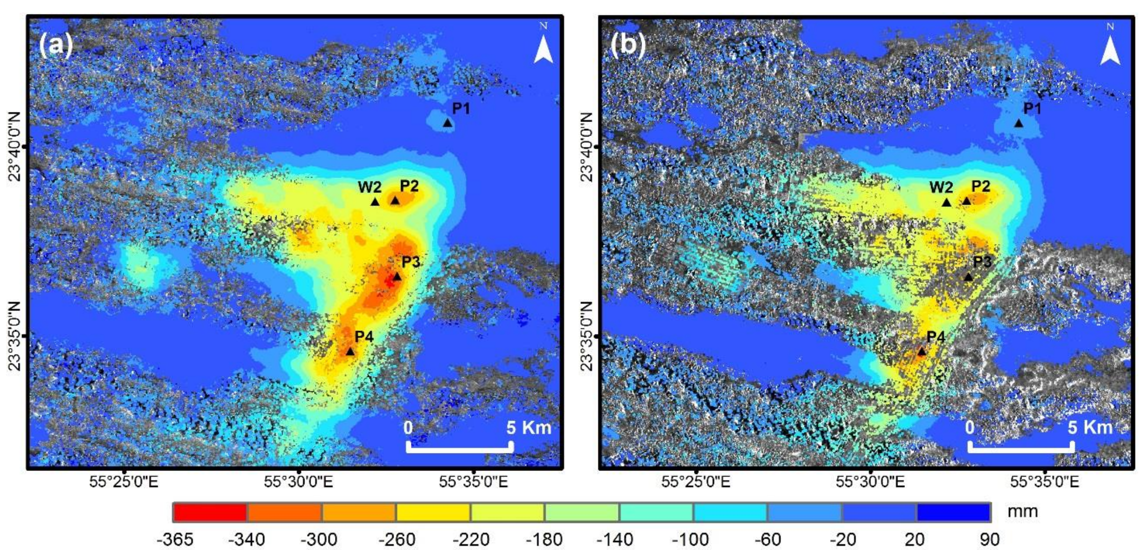

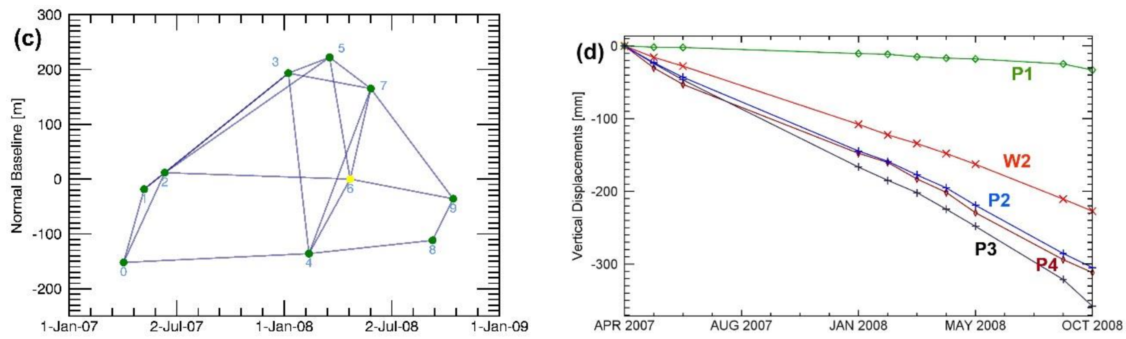

Figure 5. Comparison of the LOS displacements obtained from the two stacks with SBAS. a) Ascending stack, 3/4/2007 - 14/10/2008. b) Descending stack, 29/3/2007 - 9/10/2008. c) Time position plot of the descending stack images. d) Vertical displacement history derived from the ascending stack (3/4/2007 - 14/10/2008).

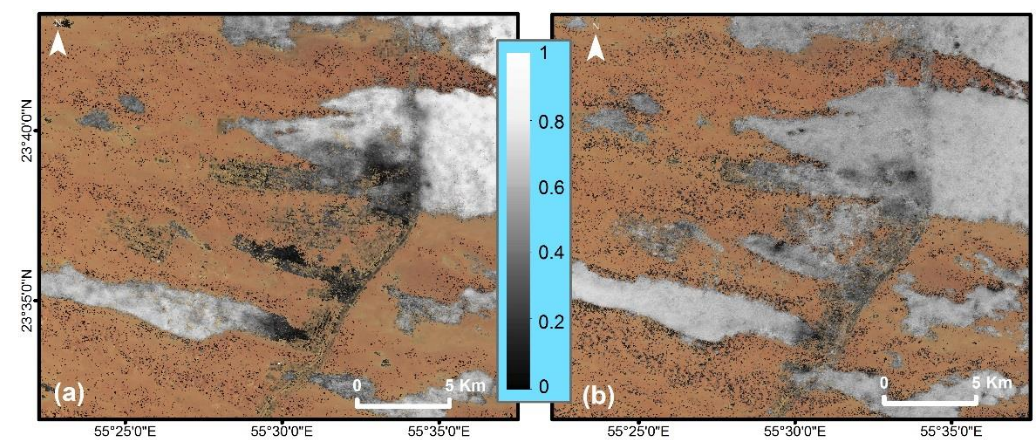

Figure 6. Multitemporal coherence. a) Descending stack. b) Ascending stack.

ALOS data

All possible interferograms within a temporal threshold of 700 days were calculated from the HH polarization images of the PALSAR acquisitions as all normal baselines were less than 2300 m. Interferograms between the FBD and FBS mode acquisitions were created after oversampling the FBD images in range to the pixel spacing of the FBS scenes (Werner et al., 2007). As it was expected, the L-band interferograms exhibited higher coherence levels and greater spatial coverage providing with a more comprehensive picture of the deformation pattern in longer time spans than the ENVISAT pairs. After the phase unwrapping stage, 16 interferograms were inverted with SBAS.

The resulting deformation maps demonstrated an almost identical subsidence pattern in terms of extent, even though non-systematic deviations were observed in comparison to the C-band derived displacement maps that locally exceeded 2 cm when compared in similar periods. Nonetheless, these differences were considered insignificant after taking into account the small number of the scenes, the subsidence magnitude and the precision of PALSAR in the achieved coherence levels (Pasquali et al., 2014). During the period 5/8/2007 – 10/8/2009, subsidence rates of 22 cm/year in the south, 21 cm/year in the central and 16 cm/year in the north farmland areas were observed from the ALOS velocity map (figure 8a).

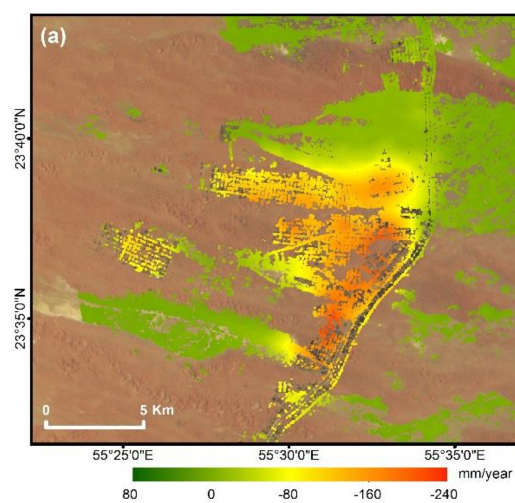

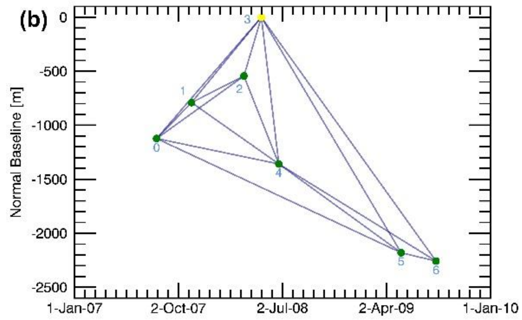

Figure 8. a) Subsidence rates obtained from the ALOS data. b) Time-baseline plot of the ALOS images.

Sentinel-1A data

The Sentinel-1A images were multilooked 8 x 2 (range x azimuth) due to the lower fringe rates and the differential interferograms (generated from the vertical polarization component) verified the continuation of the subsidence phenomenon in a similar extent but with a lower magnitude. Deformation fringes are clearly visible in pairs that include the summer season but they are not as prominent in the winter pair, indicating declining deformation trends that might have become a seasonal phenomenon, even though this is still an assumption. The generated wrapped interferograms are shown in figure 9. Results that provide stronger evidence about the recent evolution of the terrain distortions will be obtained when the number of acquisitions from Sentinel-1 will be sufficient for a time series interferometric analysis and the atmospheric artefacts in the interferograms are compensated for. Similar deformation trends were also observed in GPS data recordings of the Abu Dhabi GRS Network station of Al Wagan (personal communication with Abu Dhabi Municipality, Town Planning sector, Spatial Data Division).

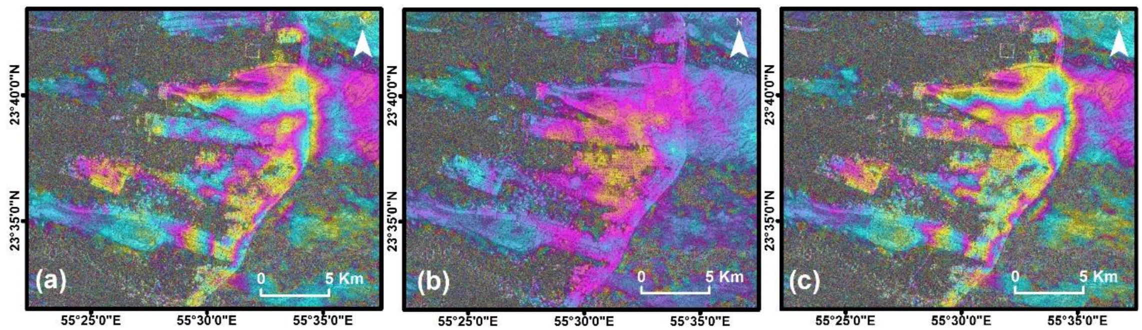

Figure 9. Differential interferograms from Sentinel-1A pairs. a) 18/2/2016 - 2/12/2016. b) 2/12/2016 - 8/3/2017. c) 18/2/2016 - 8/3/2017.

Correlation with groundwater levels

Since the subsidence phenomena in Al Wagan were attributed to water pumping from the subsurface, correlations with the groundwater levels were sought. We considered the water level data from local wells monitored by the Environmental Agency of Abu Dhabi (EAD). Even though these measurements were not concurrent and with the same frequency for all the wells, their temporal patterns was examined to define whether a relationship of the groundwater level fluctuations with the terrain deformations exists.

The groundwater elevation reduces from east to west verifying that the aquifer surface is inclined towards the west direction as mentioned in a previous study (Al Shahi, 2002). The water level time series of the wells located within the north subsiding area are generally lower contrasted to the surrounding region. This could be possibly related to groundwater extraction which had started before the sampling period, but data prior to 2000 were not available. The number of these wells is not adequate to extract conclusions about the spatial properties of the local aquifer as these should be examined in a wider area level with more similar datasets, but an indication of these spatial characteristics is locally provided.

The main observation regards the declining trends exhibited from all of the monitoring wells of the farmland area and the surroundings from 2000 and for the main period of the DInSAR observations 2003-2010. In some of the wells, a recovery trend was observed after 2012 without reaching the levels of 2000-2002, but in other cases the levels were still reducing until September 2015. Inspection of Landsat 5 and 7 imagery from 1984 - 2003 showed that the land use scenery changed dramatically during the 1990s, as it was the period of the farmland expansion. However, quantitative evidence about the start of the aquifer resource exploitation was not available. Plots of the time series of the water levels from selected representative wells are illustrated in figure 8.

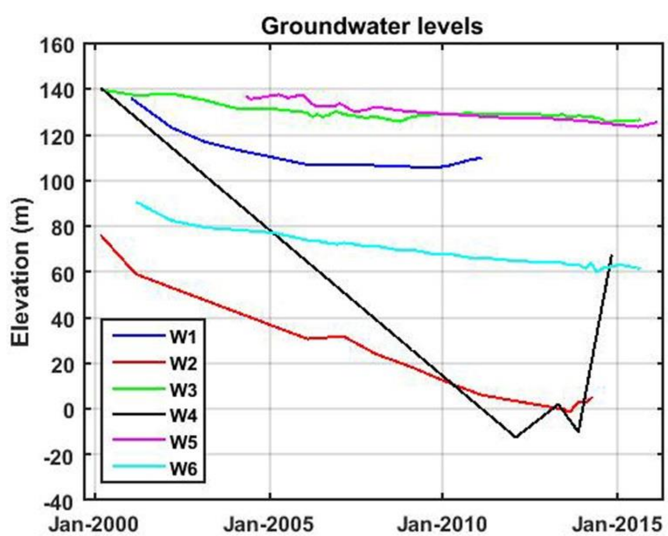

Figure 10. Groundwater levels of the monitored wells shown in figure 1a.

Conclusions

Interferometric processing over the agricultural area of Al Wagan revealed a localized subsidence phenomenon which is speculated to be groundwater related. It was observed from different sensors that subsidence velocities reached 20 cm/year during 2003-2010 with the terrain distortions exceeding -1 m. The land deformations of the study area would not have been detected if the resolution was lowered by large multilooking factors. Even though the area is not suitable for interferometric applications due to temporal decorrelation, DInSAR and SBAS techniques may still provide a terrain distortion metric if no other tools are available. The coherence maps were perfectly correlated with the land cover and the geological maps of the region, an aspect worthy of future investigation in order to define and develop the most appropriate techniques for mapping the surface deformations in the broader area of the UAE. The Sentinel-1A data verified that the surface deformation phenomena are still existent in the region constituting a potential hazard for the future.

According to the water level data, a correlation of the deformations with the groundwater resources exists. However, these data do not suffice to explain the seasonality of the subsidence pattern, while the fact that some areas are more affected than others even though the water level declinations appear similar or lower suggests that the local geology controls the phenomenon as well. The evaluation of the subsidence velocity field suggests that the loose sandy material background is more prone to terrain distortions than the compacted gravelly sediments of fluvial origin, but this also depends on the thickness of the formations. This aspect will be further sought in the geotechnical engineering properties of the different soil types of the study area by conducting in-situ sampling in the subsiding farmland area and correlating the different subsidence rates with both the aquifer resources depletion and the geophysical parameters of the varying geological background.

Another aspect that could be correlated with the deformation pattern of the farmlands and the groundwater extraction for their maintenance regards the integration of optical imagery within this study. Since the agricultural areas kept expanding during the past 20 years and the land cover changes are captured in Landsat images, this type of changes should be reflected in the vegetation indices as well. It is expected that the time series analysis of these indices for this temporal interval will be capable of providing more comprehensive explanations about the excessive use of the aquifer resources in the area and the ground deformations that were induced by this process in the study area. Future work will also include accurate GPS measurements with Global Navigation Satellite Systems (GNSS) equipment to validate the deformation time series that will be derived from the Sentinel-1A data.

References

Al-Naeem, A. A. 2014. Effect of excess pumping on groundwater salinity and water level in Hail region of Saudi Arabia. *Research Journal of Environmental Toxicology,* 8**,** 124.

Al Shahi, F. A. 2002. Assessment of Groundwater Resources in Selected Areas of Al Ain in the UAE.

Artesea, G., Fiaschib, S., Di Martirec, D., Tessitorec, S., Fabrisd, M., Achillid, V., Ahmedc, A., Borgstrome, S., Calcaterrac, D. & Ramondinif, M. 2016. Monitoring of Land Subsidence in Ravenna Municipality Using Integrated SAR-GPS Techniques: Description and First Results. *ISPRS-International Archives of the Photogrammetry, Remote Sensing and Spatial Information Sciences***,** 23-28.

Bamler, R. & Hartl, P. 1998. Synthetic aperture radar interferometry. *Inverse problems,* 14**,** R1.

Baran, I., Stewart, M. & Claessens, S. 2005. A new functional model for determining minimum and maximum detectable deformation gradient resolved by satellite radar interferometry. *IEEE Transactions on Geoscience and Remote Sensing,* 43**,** 675-682.

Berardino, P., Fornaro, G., Lanari, R. & Sansosti, E. 2002. A new algorithm for surface deformation monitoring based on small baseline differential SAR interferograms. *IEEE Transactions on Geoscience and Remote Sensing,* 40**,** 2375-2383.

Bürgmann, R., Rosen, P. A. & Fielding, E. J. 2000. Synthetic aperture radar interferometry to measure Earth's surface topography and its deformation. *Annual review of earth and planetary sciences,* 28**,** 169-209.

Cantone, A., Riccardi, P., Baker, H., Pasquali, P., Closson, D. & Karaki, N. A. Monitoring Small land Subsidence Phenomena in the Al-Ain Region by Satellite SAR Interferometric Stacking. Second EAGE International Conference on Engineering Geophysics, 2013.

Chaussard, E., Wdowinski, S., Cabral-Cano, E. & Amelung, F. 2014. Land subsidence in central Mexico detected by ALOS InSAR time-series. *Remote sensing of environment,* 140**,** 94-106.

Environmental Agency of Abu Dhabi 2009. Abu Dhabi Water Resources Masterplan.

Ferretti, A. 2014. *Satellite InSAR data: reservoir monitoring from space*, EAGE Publications.

Ferretti, A., Prati, C. & Rocca, F. 2000. Nonlinear subsidence rate estimation using permanent scatterers in differential SAR interferometry. *IEEE Transactions on geoscience and remote sensing,* 38**,** 2202-2212.

Ferretti, A., Prati, C. & Rocca, F. 2001. Permanent scatterers in SAR interferometry. *IEEE Transactions on geoscience and remote sensing,* 39**,** 8-20.

Goldstein, R. M. & Werner, C. L. 1998. Radar interferogram filtering for geophysical applications. *Geophysical research letters,* 25**,** 4035-4038.

Gonzalez, R., Ouarda, T. B.M.J., Marpu, P. R., Allam, M. M., Eltahir, E. A. & Pearson, S. 2016. Water Budget Analysis in Arid Regions, Application to the United Arab Emirates. *Water,* 8**,** 415.

Holzer, T. L. & Galloway, D. L. 2005. Impacts of land subsidence caused by withdrawal of underground fluids in the United States. *Reviews in Engineering Geology,* 16**,** 87-99.

Hooper, A., Zebker, H., Segall, P. & Kampes, B. 2004. A new method for measuring deformation on volcanoes and other natural terrains using InSAR persistent scatterers. *Geophysical research letters,* 31.

Kim, J.-W., Lu, Z., Jia, Y. & Shum, C. 2015. Ground subsidence in Tucson, Arizona, monitored by time-series analysis using multi-sensor InSAR datasets from 1993 to 2011. *ISPRS Journal of Photogrammetry and Remote Sensing,* 107**,** 126-141.

Lanari, R., Casu, F., Manzo, M., Zeni, G., Berardino, P., Manunta, M. & Pepe, A. 2007. An overview of the small baseline subset algorithm: A DInSAR technique for surface deformation analysis. *Pure and Applied Geophysics,* 164**,** 637-661.

Lanari, R., Mora, O., Manunta, M., Mallorquí, J. J., Berardino, P. & Sansosti, E. 2004. A small-baseline approach for investigating deformations on full-resolution differential SAR interferograms. *IEEE Transactions on Geoscience and Remote Sensing,* 42**,** 1377-1386.

Massonnet, D. & Feigl, K. L. 1998. Radar interferometry and its application to changes in the Earth's surface. *Reviews of geophysics,* 36**,** 441-500.

Pasquali, P., Cantone, A., Riccardi, P., Defilippi, M., Ogushi, F., Gagliano, S. & Tamura, M. 2014. Mapping of Ground Deformations with Interferometric Stacking Techniques. *Land Applications of Radar Remote Sensing.* InTech.

Pepe, A. & Lanari, R. 2006. On the extension of the minimum cost flow algorithm for phase unwrapping of multitemporal differential SAR interferograms. *IEEE Transactions on Geoscience and remote sensing,* 44**,** 2374-2383.

Statistics Centre of Abu Dhabi 2014. Agricultural land uses 2013 Statistical Report.

Strozzi, T., Wegmuller, U., Tosi, L., Bitelli, G. & Spreckels, V. 2001. Land subsidence monitoring with differential SAR interferometry. *Photogrammetric engineering and remote sensing,* 67**,** 1261-1270.

Vrba, J. 2003. The impact of aquifer intensive use on groundwater quality. *Intensive use of groundwater. Challenges and opportunities***,** 113-132.

Werner, C., Wegmüller, U., Strozzi, T., Wiesmann, A. & Santoro, M. PALSAR multi-mode interferometric processing. Proc. First Joint PI Symp. ALOS Data Nodes for ALOS Sci. Program, 2007. 19-23.

Yagoub, M. M. 2015. Spatio-temporal and hazard mapping of Earthquake in UAE (1984–2012): Remote sensing and GIS application. *Geoenvironmental Disasters,* 2**,** 13.